$LiMn_2O_4$ microspheres secondary structure of nanoparticles/plates as cathodes for Li-ion batteries

Cheng-Yue Sun, Yun-Guang Zhu, Tie-Jun Zhu,[a] Jian Xie, Gao-Shao Cao, and Xin-Bing Zhao
State Key Laboratory of Silicon Materials; Key Laboratory of Advanced Materials and Applications for Batteries of Zhejiang Province; and Department of Materials Science and Engineering, Zhejiang University, Hangzhou 310027, China

Shi-Chao Zhang
School of Materials Science and Engineering, Beijing University of Aeronautics and Astronautics, Beijing 100191, China

(Received 2 December 2012; accepted 26 March 2013)

In this work, we succeeded in synthesis of spinel $LiMn_2O_4$ via a facile self-template method. The product displays a micro-/nanohybrid structure. Nanoparticles/plates act as the primary nanoblocks to build the secondary microarchitecture. There is the open space between the nanoblocks and the void space between the secondary structures. Electrochemical tests demonstrate that the as-synthesized sample exhibits superior rate capability and high-rate cycleability when contrasted with its solid counterpart. The initial discharge capacity is 126 mAh/g at 0.1 C, 110 mAh/g at 10 C, and 84 mAh/g at 20 C. The discharge capacity retention of about 80% is obtained after 800 cycles at 10 C. The high capacity and excellent cycling life of the material shows its potential for application as high-power batteries. The improved rate capability and cycleability can be attributed to its secondary structure that can facilitate fast Li-insertion/extraction and buffer the volume expansion/contraction upon cycling.

I. INTRODUCTION

With great success in portable electric devices, lithium ion batteries (LIBs) have been considered as the most promising energy storage devices.[1–3] However, there are persistent demands for batteries with higher power density and longer cycling life to power newly emerging devices. Among the various cathode materials being evaluated for high-power, high-performance LIBs such as lithium-cobalt oxide (LCO), lithium-manganese oxide (LMO), lithium-iron phosphate (LFP), lithium-nickel-manganese-cobalt oxide (NMC), and lithium nickel-cobalt-aluminum oxide (LCA), the cathode material lithium manganese oxide ($LiMn_2O_4$), also known as LMO, is one of the most promising candidates due to its low cost, environmental friendliness, and abundant availability.[4–6] In spite of $LiMn_2O_4$ having many merits, its power performance and cycling stability are often hampered by problems of large polarization and capacity decay especially under large currents.[7–9] The large polarization is generally considered to be due to sluggish Li^+ diffusion in bulk electrode, and the capacity decay often results from manganese (Mn) dissolution or structure transformation.[10–12] To overcome the demerits, various strategies have been implemented such as: (i) decreasing the particle size to nanoscale, (ii) resorting to surface coating and (iii) cations doping. However, surface coating and cations doping are at the expense of yieldable capacity.[13,14] Compared with the bulk counterpart, the nanoscaled electrode materials can shorten Li^+ diffusion distance and facilitate faster Li^+ migration, resulting in better high-rate performance.[15,16] Hence, design and synthesis of nanosized cathodes can be a very efficient solution.

Recently, great attention has been paid to the electrode materials with secondary architecture built by primary nanoblocks. The hierarchical structure will enhance the electrode/electrolyte contact area, shorten the Li^+ diffusion length; the void space between neighboring nanoblocks allows easy diffusion of the electrolyte; and secondary architecture built by primary nanoblocks can buffer strain from volume variation during Li insertion/extraction.[17] For example, the composite of Sn/C (tin nanoparticles as encapsulated in elastic hollow carbon spheres) exhibits a capacity of over 550 mAh/g after 100 cycles.[18] Lee et al.[19] reported the hollow sphere built upon by lithium iron phosphate, also known as LFP, nanoparticles ($C/LiFePO_4$) with a secondary architecture built by primary nanoblocks and improved electrochemical performance. Deng et al.[20] have reported that core-shelled mesospheres of SnO_2 nanoparticles could exhibit a high Li-storage capacity.

In this work, we prepared $LiMn_2O_4$ microspheres secondary structure of nanoparticles/plates via a facile template-support reaction. To our knowledge, there are no reports on the synthesis of the $LiMn_2O_4$ with this secondary structure as cathodes for LIBs. The material may have some structural advantages for the application in LIBs. First, primary nanoblocks in this structure can

[a]Address all correspondence to this author.
e-mail: zhutj@zju.edu.cn
DOI: 10.1557/jmr.2013.84

 © Materials Research Society 2013

https://doi.org/10.1557/jmr.2013.84 Published online by Cambridge University Press

process fast Li^+ insertion/extraction due to reduced diffusion distance, which may result in improved rate capability. Additionally, the secondary structure can buffer the volume changes and keep in tact structural stability during cycling, displaying improved cycling performance. As expected, compared with the solid counterpart, the sample with secondary structure displays remarkably improved performance in terms of high discharge capacity, excellent rate capability and long cycling life.

II. EXPERIMENTAL

All the chemicals were used without further purification. Manganese carbonate ($MnCO_3$) microspheres were prepared by the precipitation method.[21] Manganese sulfate ($MnSO_4$) (4 mmol) was dissolved in 200 mL of distilled water. Then, 40 mL of ethanol was added in the above solution under stirring. In the successive step, 200 mL of ammonium bicarbonate (NH_4HCO_3) solution (0.2 M) was slowly dropped into the mixed solution under stirring. After the reaction, the white precipitate was collected, washed with distilled water and ethanol repeatedly and dried at 50 °C under vacuum for 12 h. The $LiMn_2O_4$ microspheres secondary structure of nanoparticles/plates (CSPMS-LMO) was prepared as follows: first, the obtained $MnCO_3$ microspheres were precalcined at 500 °C for 4 h to form hierarchical Mn_2O_3; second, MnO_2 microspheres secondary structure of nanoparticles/plates (CSPMS-MO) were obtained by etching Mn_2O_3 with 0.45 M HCl; finally, CSPMS-LMO was prepared by calcining CSPMS-MO with LiOH at 700 °C for 8 h in air. For comparison, solid $LiMn_2O_4$ microspheres (SM-LMO) were also prepared by the same solid-state reaction using the prepared $MnCO_3$ and LiOH as precursors.

The crystalline structure of the samples was characterized by x-ray diffraction on (XRD; Rigaku model No. D/Max-2550pc, Rigaku Industrial Corporation, Osaka, Japan) powder diffractometer. The chemical compositions of the product were determined by inductively coupled plasma-atomic emission spectrometry (ICP-AES; IRIS Intrepid II XSP, Thermo Electron Corporation, Waltham, MA). The morphologies were observed by on (FESEM; FEI-sirion microscope) and transmission electron microscopy on a microscope (TEM; model No. JEM 2100F, JEOL Ltd., Tokyo, Japan). The specific surface area of the products was determined by the Brunauer-Emmett-Teller (BET) method.

The electrochemical properties of the samples were evaluated with CR2025-type coin cells. The electrode slurry was made by blending 80 wt% active materials, 10 wt% acetylene black (AB) and 10 wt% polyvinylidene fluoride (PVDF) in N-methyl pyrrolidone (NMP). The slurry was then coated onto Al foil to make the working electrodes followed by drying at 80 °C under vacuum for 12 h. The cells were assembled in an argon-filled glove box using metallic Li foil as the counter electrode, 1 M lithium hexafluorophosphate ($LiPF_6$) in ethylene carbonate (EC)-dimethyl carbonate (DMC) (1:1 in volume) as the electrolyte, and polypropylene microporous film (Celgard 2300, Celgard LLC Corporate, Charlotte, NC) as the separator. Galvanostatic charge/discharge was performed on a BTS battery tester (Neware, Shenzhen, China) in the voltage range of ~3.5–4.3 V at various current densities. Cycle voltammetry (CV) tests were carried out on a CHI 660C electrochemistry workstation (Chenhua Instrument Co, Shanghai, China) at 0.1 mV/s.

III. RESULTS AND DISCUSSION

In Fig. 1(a), all the diffraction peaks of the product can be indexed to a cubic spinel phase of $LiMn_2O_4$ [Joint Committee on Powder Diffraction Standards (JCPDS) No. 35-0782]. No other additional peaks of possible impurities of Mn_2O_3 or Li_2MnO_3 are observed. Chemical composition of the product was further analyzed by ICP-AES. The result shows the atomic ratio of Li/Mn is 1.06:2. It displays the formation of lithium-rich spinel-type lithium manganese oxide phase and lithium may occupy some manganese sites (16c) in the spinel lattice.[16] The microspheres have a diameter of around 7 μm [Fig. 1(b)]. Figure 1(c) displays further magnification image of the broken microsphere. We can observe that nanoparticles/plates are used as nanoblocks to assemble secondary microspheres. The product may have some structure advantages for LIBs. First, the secondary structure may provide a facile route of Li^+ moving. Besides, the primary nanoplates/particles can short the distance of Li^+ diffusion. Finally, the secondary microspheres may buffer volume variation and exhibit superior structure stability. From high-resolution transmission electron microscopy (HRTEM) image in Fig. 1(d), the measured *d*-spacing of 0.48 nm is consistent with that of (111) plane of $LiMn_2O_4$, confirming a good crystallization of the product.

The formation of spinel $LiMn_2O_4$ includes four steps: the preparation of the precursor $MnCO_3$, suitable precalcination, washing with HCl and high-temperature lithiation. From the XRD pattern in Fig. 2(a), the product obtained by the precipitation method can be indexed to single phase $MnCO_3$ (JCPDS No. 44-1472). After precalcination at 500 °C for 4 h, all the diffraction peaks can be indexed to single Mn_2O_3, and no peaks of other phases such as $MnCO_3$ or MnO_2 are observed [Fig. 2(b)]. After washing Mn_2O_3 with 0.45 M HCl, typical peaks of hexagonal MnO_2 are detected obviously, such as (100), (101), (110) and (102) peaks, consistent with JCPDS No. 30-0820 [Fig. 2(c)]. There are other obvious diffraction peaks that can be observed. From Figs. 2(b) and 2(c), we can see that the transformation from Mn_2O_3 into MnO_2 occur by washing Mn_2O_3 with HCl. It is suggested that the disproportionation reaction ($2Mn^{3+} \rightarrow Mn^{2+} + Mn^{4+}$) may take place during washing with HCl. The product MnO may preferentially

https://doi.org/10.1557/jmr.2013.84 Published online by Cambridge University Press

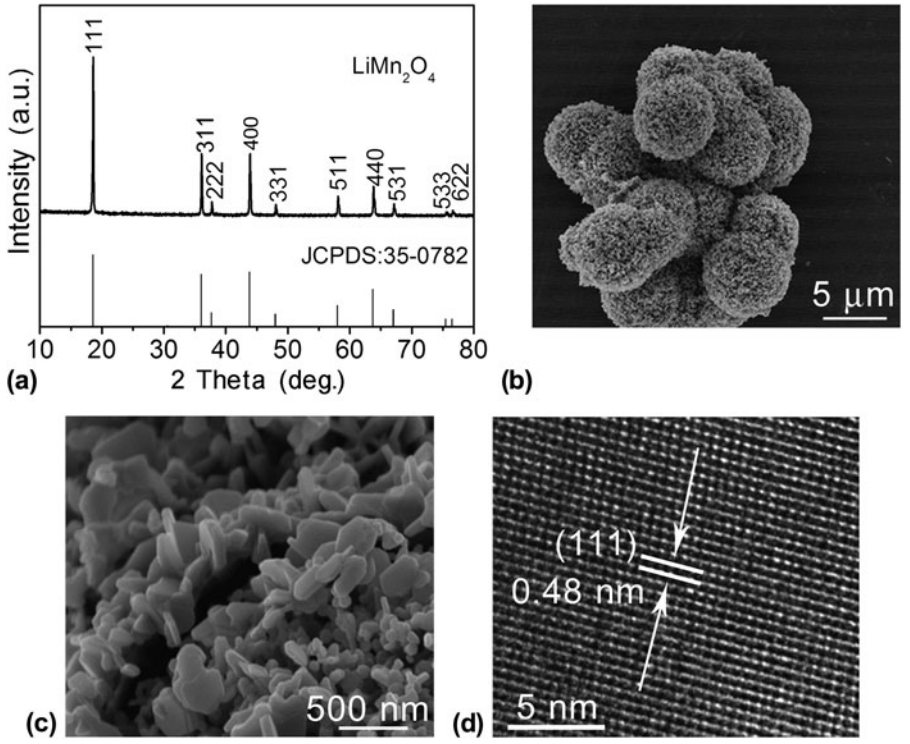


FIG. 1. (a) XRD pattern of as-synthesized $LiMn_2O_4$; morphology of the product: (b) low-magnification SEM image, (c) high-magnification SEM images of a broken microsphere, (d) HRTEM image of a nanoplate.

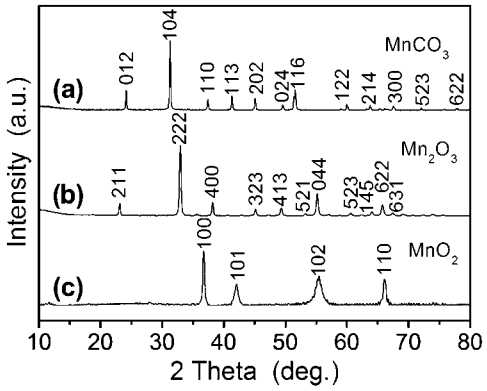


FIG. 2. XRD patterns of (a) $MnCO_3$ prepared by the precipitation method, (b) hierarchical Mn_2O_3 obtained after precalcination of $MnCO_3$ at 500 °C for 4 h, (c) MnO_2 obtained after etching Mn_2O_3 using 0.45 M HCl.

dissolve into HCl. But it is very difficult for MnO_2 to dissolve into dilute HCl at room temperature. Therefore, the remaining solid product is MnO_2 after washing Mn_2O_3 with HCl. Besides, to further confirm whether the transformation from Mn_2O_3 to MnO_2 takes place, we calculated the weight loss of the solid after HCl etching. The weight loss of the solid is calculated to be 46%, related to the dissolution of MnO (45%). This can also confirm that the transformation from Mn_2O_3 to MnO_2, in fact, did take place.

The uniform $MnCO_3$ microspheres with the diameter of about 9 μm are formed during the precipitation reaction [Fig. 3(a)]. The surface of microspheres consists of nanopyramids [the inset in Fig. 3(a)]. In Fig. 3(b), solid microsphere exhibits different structures between inner core and outer shell. The inner core displays a closed-packed structure marked by an inner dotted circle, while the outer shell presents a radial structure marked by an outer dotted circle. Interestingly, after precalcination and washing, a three-dimensional microarchitecture is formed with nanoparticles/plates as primary nanoblocks. In Figs. 3(c) and 3(d), the diameter of MnO_2 microspheres is around 7 μm, composed of nanoplates and nanoparticles. Upon precalcination, $MnCO_3$ is oxidized to Mn_2O_3. In the successive step, we use diluted HCl to wash Mn_2O_3 microspheres. Mn^{3+} takes part in a disproportionation reaction ($2Mn^{3+} \rightarrow Mn^{2+} + Mn^{4+}$). According to "Kirkendall effect," movement of interface between diffusion couples (Mn^{2+}/Mn^{4+}) can contribute to the formation of primary nanoblocks.[22] At the same time, MnO preferentially dissolves into HCl, while MnO_2 forms the solid interface because it is difficult for MnO_2 to dissolve into diluted HCl at room temperature. Therefore, we prepare the CSPMS-MO with nanoparticles/plates as primary nanoblocks. In the successive step, CSPMS-MO is used as self-support template and calcined with LiOH to obtain the target product $LiMn_2O_4$.

Coin-type cells were used to evaluate the electrochemical performance of $LiMn_2O_4$ samples (CSPMS-LMO and SM-LMO). Figure 4(a) displays the first charge/discharge curves of two samples at C/10 rate (1 C = 148 mA/g). Two plateaus are clearly seen in both samples, corresponding to

https://doi.org/10.1557/jmr.2013.84 Published online by Cambridge University Press

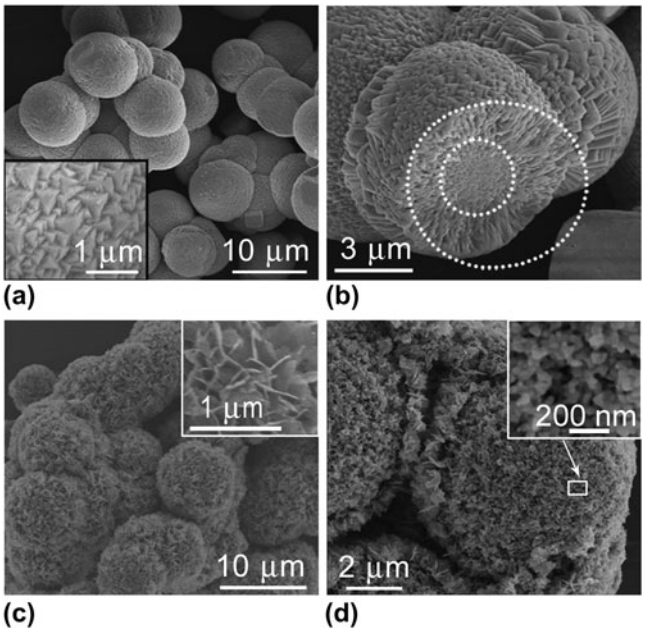


FIG. 3. Morphology of (a) $MnCO_3$ microspheres prepared by the precipitation method, the inset shows the outer surface of a microsphere, (b) a cross-sectional view of the broken $MnCO_3$ microsphere, (c) MnO_2 obtained after etching Mn_2O_3 with 0.45 M HCl, the inset shows the surface of the microsphere, (d) broken microspheres of MnO_2, the inset shows the magnifying image of the section as marked by white pane.

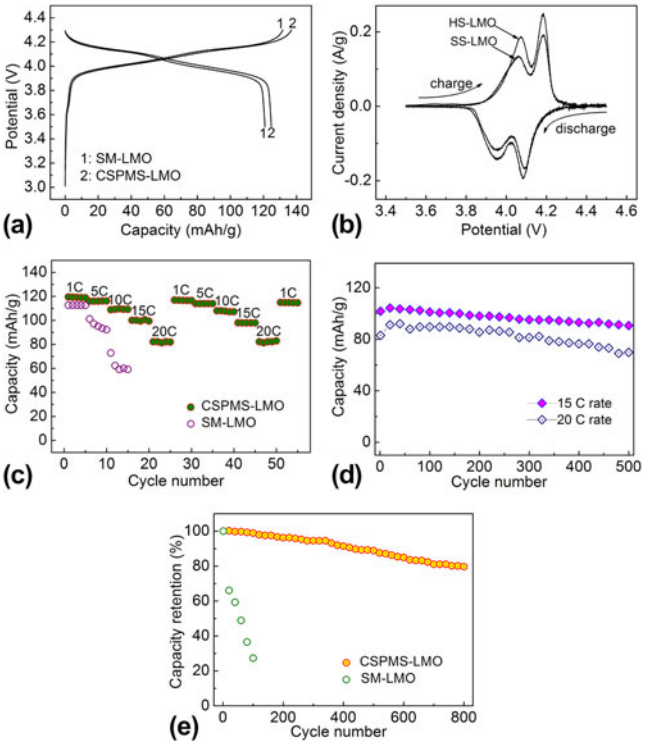


FIG. 4. (a) The first charge/discharge curves of CSPMS-LMO and SM-LMO, (b) CV plots at 0.1 mV/s between 3.4 and 4.6 V, (c) the comparison of rate capability between CSPMS-LMO and SM-LMO, (d) discharge capacity as a function of cycle number for CSPMS-LMO electrode at different rates, (e) the comparison of cycling stability between CSPMS-LMO and SM-LMO at 10 C.

the two-step Li-insertion/extraction mechanism.[23] But CSPMS-LMO/Li cell displays the first discharge capacity of 126 mAh/g, slightly higher than that of SM-LMO/Li cell (119 mAh/g). It may be due to that the microspheres with secondary structure have larger surface area (18.3 m^2/g), more than that of solid microspheres (3.8 m^2/g). The large surface area can enhance active-material/electrolyte contact area and facilitate the redox reactions. From CV curves [Fig. 4(b)], two pairs of redox peaks are well defined, which agree well with the two pairs of potential plateaus in the charge/discharge curves. Remarkably, the peaks of CSPMS-LMO electrode are sharper than those of SM-LMO. This reveals higher crystalline of CSPMS-LMO. It also indicates superior reversibility of Li^+ transport in its bulk and through its interface with the electrolyte.[16]

To explore power performance of the samples, rate capabilities of two samples were compared [Fig. 4(c)]. Obviously, CSPMS-LMO electrode displays rather better rate capability than SM-LMO electrode. The discharge capacity of CSPMS-LMO/Li cell can be recovered to 118 mAh/g when the current decreases from 20 to 1 C, indicating good reversibility. Although the discharge capacity decreases with increasing current density, the discharge capacities of 115 and 84 mAh/g are still retained at 10 and 20 C. Near 71% of its capacity can be preserved when the current increases from 1 to 20 C rate. The capacity loss can be explained by the ohmic drop and increased cell polarization at high current densities.[15] It is also suggested that the capacity loss observed on the increased rate is due to kinetic limitations, but not due to some structural changes of electrode materials. Our values are also higher than those of $LiMn_2O_4$ nanotubes (80 mAh/g at 10 C)[16] and $LiMn_2O_4$ hollow microspheres (60 mAh/g at 3.4 C).[24] It is hypothesized that the secondary microspheres may have more structural advantages when compared with that of nanotubes and hollow microspheres, such as higher electrochemical activity, easier penetration of the electrolyte and fast Li^+ moving. The superior power performance of CSPMS-LMO can be attributed to its unique structure. First, the CSPMS-LMO can supply a large surface area due to assembled microarchitecture, which facilitates the redox reactions. Second, primary nanoblocks can shorten Li^+ diffusion distance. It is beneficial for fast Li^+ insertion/extraction and can result in good rate capability. When electrode material is discharged at 1, 5, and 10 C, the discharge capacities are 120, 115, and 110 mAh/g. Our values are higher than those of $LiMn_2O_4$ electrodes obtained by coprecipitation method (63 mAh/g at 3 C),[25] combustion reaction (73 mAh/g at 1 C),[26] and hydrothermal method (117 mAh/g at 0.5 C).[27] The better electrochemical properties can be ascribed to template-engaged synthesis method,

https://doi.org/10.1557/jmr.2013.84 Published online by Cambridge University Press

which can prepare the product with high crystallinity and secondary structure.

To investigate the high-rate cycleability of CSPMS-LMO, the material was discharged at 15 and 20 C after charging at 1 C rate [Fig. 4(e)]. The initial discharge capacities are 102 and 84 mAh/g. CSPMS-LMO electrode can still maintain discharge capacities of 91 and 70 mAh/g at 15 and 20 C after 500 cycles, revealing superior high-rate cycleability. It is suggested that microarchitecture built by nanoblocks can buffer the volume changes of the material upon repeated cycling, which is beneficial for sustaining structural stability and keeping high capacities even after 500 cycles.[19,28] To further distinguish this secondary-structure electrode and solid counterpart, the cycleability was further investigated both CSPMS-LMO and SM-LMO electrodes at 10 C discharge rate. It is apparent that the CSPMS-LMO electrode displays much better cycling stability compared with the SM-LMO electrode [Fig. 4(e)]. The capacity retention of 80% can be obtained after 800 cycles for CSPMS-LMO electrode. By contrast, the SM-LMO electrode can keep only 20% of its initial capacity after 100 cycles. Notably, CSPMS-LMO electrodes supply a better cycleablity in contrast with their solid counterpart. This is due to the fact that primary nanoblocks can shorten Li^+ diffusion distance and facilitate rapid Li^+ moving in the actives. This can decrease polarization during charge/discharge and result in superior cycling behavior.

IV. CONCLUSIONS

In summary, we succeeded in designing and synthesizing $LiMn_2O_4$ microspheres secondary structure of nanoparticles/plates by a template-engaged method. As cathodes for LIBs, the product shows much improved rate capability and cycling life in contrast to their solid counterpart. The remarkably enhanced performance can be ascribed to the secondary structure of the product, which is beneficial for fast Li-insertion/extraction and buffering the volume expansion/contraction upon cycling. In view of facile fabrication and improved performance, this material shows a promising application as cathodes for LIBs aiming for high-power applications.

ACKNOWLEDGMENTS

The authors appreciate the support from National Basic Research Program of China (Grant No. 2013CB934001), the National Natural Science Foundation of China (Grant No. 51101139), the Ph.D. Programs Foundation of Ministry of Education of China (Grant No. 20100101120024), the Qianjiang Talents Project of Science Technology Department of Zhejiang Province (Grant No. 2011R10021), and Key Science and Technology Innovation Team of Zhejiang Province under Grant No. 2010R50013.

REFERENCES

1. B. Scrosati: Challenge of portable power. *Nature* **373**, 557 (1995).
2. J. Marier: Nanoionics: Ion transport and electrochemical storage in confined systems. *Nat. Mater.* **4**, 805 (2005).
3. S.Y. Chung, J.T. Bloking, and Y.M. Chiang: Electronically conductive phospho-olivines as lithium storage electrodes. *Nat. Mater.* **1**, 123 (2002).
4. W. Li, J.R. Dahn, and D.S. Wainwright: Rechargeable lithium batteries with aqueous electrolytes. *Science* **264**, 1117 (1994).
5. M.S. Whittingham: Materials challenges facing electrical energy storage. *Mater. Res. Bull.* **33**, 411 (2008).
6. M.M. Thackeray, P.J. Johnson, L.A. Depicciotto, P.G. Bruce, and J.B. Goodenough: Electrochemical extraction of lithium from $LiMn_2O_4$. *Mater. Res. Bull.* **19**, 179 (1984).
7. M.M. Thackeray: Structural considerations of layered and spinel lithium ion batteries. *J Electrochem. Soc.* **142**, 2558 (1995).
8. F. Jiao, K.M. Shaju, and P.G. Bruce: Synthesis of nanowire and mesoporous low-temperature $LiCoO_2$ by a post-templating reaction. *Angew. Chem. Int. Ed.* **44**, 6550 (2005).
9. W. Tang, S. Tian, L.L. Liu, L. Li, H.P. Zhang, Y.B. Yue, Y. Bai, Y.P. Wu, and K. Zhu: Nano-$LiCoO_2$ as cathode material of large capacity and high rate capability for aqueous rechargeable lithium batteries. *Electrochem. Commun.* **12**, 1524 (2010).
10. Y. Wang and G. Cao: Developments in nanostructured cathode materials for high-performance lithium-ion batteries. *Adv. Mater.* **20**, 2251 (2008).
11. Y.G. Guo, Y.S. Hu, W. Sigle, and J. Marier: Superior electrode performance of nanostructured mesoporous TiO_2 (Anatase) through efficient hierarchical mixed conducting networks. *Adv. Mater.* **19**, 2087 (2007).
12. Y.L. Ding, J. Xie, G.S. Cao, T.J. Zhu, H.M. Yu, and X.B. Zhao: Enhanced elevated-temperature performance of Al-doped single-crystalline $LiMn_2O_4$ nanotubes as cathodes for lithium ion batteries. *J. Phys. Chem. C* **115**, 9821 (2011).
13. L.J. Fu, T. Zhang, Q. Cao, H.P. Zhang, and Y.P. Wu: Preparation and characterization of three-dimensionally ordered mesoporous titania microparticles as anode material for lithium ion battery. *Electrochem. Commun.* **9**, 2143 (2007).
14. J.C. Lytle, H. Yan, N.S. Ergang, W.H. Smyrl, and A. Stein: Structural and electrochemical properties of three-dimensionally ordered macroporous tin(IV) oxide films. *J. Mater. Chem.* **14**, 1621 (2004).
15. E. Hosono, T. Kudo, I. Honma, H. Matsuda, and H. Zhou: Synthesis of single crystalline spinel $LiMn_2O_4$ nanowires for a lithium ion battery with high power density. *Nano Lett.* **9**, 1045 (2009).
16. Y.L. Ding, J. Xie, G.S. Cao, T.J. Zhu, H.M. Yu, and X.B. Zhao: Single-crystalline $LiMn_2O_4$ nanotubes synthesized via template-engaged reaction as cathodes for high-power lithium ion batteries. *Adv. Funct. Mater.* **21**, 348 (2011).
17. L. Hu, H. Zhong, X. Zheng, Y. Huang, P. Zhang, and Q. Chen: $CoMn_2O_4$ spinel hierarchical microspheres assembled with porous nanosheets as stable anodes for lithium-ion batteries. *Sci. Rep.* **2**, 986 (2012).
18. W.M. Zhang, J.S. Hu, Y.G. Guo, S.F. Zheng, L.S. Zhong, W.G. Song, and L.J. Wan: Tin-nanoparticles encapsulated in elastic hollow carbon spheres for high-performance anode material in lithium-ion batteries. *Adv. Mater.* **20**, 1160 (2008).
19. M.H. Lee, J.Y. Kim, and H.K. Song: A hollow sphere secondary structure of $LiFePO_4$ nanoparticles. *Chem. Mater.* **46**, 6795 (2010).
20. D. Deng and J.Y. Lee: Hollow core-shell mesospheres of crystalline SnO_2 nanoparticle aggregates for high capacity Li^+ ion storage. *Chem. Mater.* **20**, 1841 (2008).
21. J. Fei, Y. Cui, X. Yan, W. Qi, Y. Yang, K. Wang, Q. He, and J. Li: Controlled preparation of MnO_2 hierarchical hollow nanostructures and their application in water treatment. *Adv. Mater.* **20**, 452 (2008).

https://doi.org/10.1557/jmr.2013.84 Published online by Cambridge University Press

22. J. Cao, Y. Zhu, L. Shi, L. Zhu, K. Bao, S. Liu, and Y. Qian: Double-shelled Mn_2O_3 hollow spheres and their application in water treatment. *Eur. J. Inorg. Chem.* **2010**, 1172 (2010).
23. Y. Xia and M. Yoshio: An investigation of lithium ion insertion into spinel structure Li-Mn-O compounds. *J. Electrochem. Soc.* **143**, 825 (1996).
24. X. Xiao, J. Lu, and Y. Li: $LiMn_2O_4$ microspheres: Synthesis, characterization and use as a cathode in lithium ion batteries. *Nano Res.* **3**, 733 (2010).
25. A.R. Naghash and J.Y. Lee: Preparation of spinel lithium manganese oxide by aqueous co-precipitation. *J. Power Sources* **85**, 284 (2000).
26. D. Kovacheva, H. Gadjov, K. Petrov, S. Mandal, M.G. Lazarraga, L. Pascual, J.M. Amarilla, R.M. Rojas, P. Herrero, and J.M. Rojo: Synthesizing nanocrystalline $LiMn_2O_4$ by a combustion route. *J. Mater. Chem.* **12**, 1184 (2002).
27. H.M. Wu, J.P. Tu, Y.F. Yuan, X.T. Chen, J.Y. Xiang, X.B. Zhao, and G.S. Cao: One-step synthesis $LiMn_2O_4$ cathode by a hydrothermal method. *J. Power Sources* **161**, 1260 (2006).
28. L. Zhou, H.B. Wu, T. Zhu, and X.W. Lou: Facile preparation of $ZnMn_2O_4$ hollow microspheres as high-capacity anodes for lithium-ion batteries. *J. Mater. Chem.* **22**, 827 (2012).

https://doi.org/10.1557/jmr.2013.84 Published online by Cambridge University Press